Available online at www.sciencedirect.com

ScienceDirect

Procedia Computer Science 239 (2024) 2278–2285

Procedia Computer Science

www.elsevier.com/locate/procedia

CENTERIS – International Conference on ENTERprise Information Systems / ProjMAN – International Conference on Project MANagement / HCist – International Conference on Health and Social Care Information Systems and Technologies 2023

Landslide velocity mapping using ALOS-2 PALSAR-2 ScanSAR data

Urs Wegmüller, Christophe Magnard*, Tazio Strozzi, Rafael Caduff, Nina Jones

Gamma Remote Sensing AG, Worbstrasse 225, CH-3073 Gümligen, Switzerland

Abstract

This work discusses landslide velocity mapping in the Swiss Alps using ALOS-2 PALSAR-2 ScanSAR differential interferometry and interferometric time series analyses based on small data stacks of about 10 images over eight years. A wide area coverage is possible due to the 350km swath width of the ScanSAR data. In our processing sequence we resampled the sub-swath SLCs to a common spatial grid. The co-registered sub-swath SLCs were mosaiced into large co-registered mosaic SLCs. We then applied normal procedures also used for stripmap mode data to generate differential interferograms and conduct a Persistent Scatterer Interferometry (PSI) processing. The results obtained over the Swiss Alps provide a good spatial coverage, with line-of-sight displacement velocities also extracted for some landslides in forested areas. The future applicability of the technique is very promising with upcoming L-band SAR missions (NISAR, ROSE-L and PALSAR-3) that provide data of even better suitability – higher spatial resolution, shorter revisit time intervals, and free and open data access.

© 2024 The Authors. Published by Elsevier B.V.
This is an open access article under the CC BY-NC-ND license (https://creativecommons.org/licenses/by-nc-nd/4.0)
Peer-review under responsibility of the scientific committee of the CENTERIS / ProjMAN / HCist 2023

Keywords: Satellite L-band SAR; DInSAR; PSI; SBAS; time-series analysis; SAR interferometry; displacement monitoring; landslides; ground-motion; ScanSAR.

* Corresponding author. Tel.: +41-31-9517005 .
E-mail address: magnard@gamma-rs.ch

1877-0509 © 2024 The Authors. Published by Elsevier B.V.
This is an open access article under the CC BY-NC-ND license (https://creativecommons.org/licenses/by-nc-nd/4.0)
Peer-review under responsibility of the scientific committee of the CENTERIS / ProjMAN / HCist 2023
10.1016/j.procs.2024.06.419

1. Introduction

Interferometric Synthetic Aperture Radar (InSAR) based methods play an increasingly important role in different phases of the management of gravitational natural hazards, e.g., in Switzerland [1]. The two main requirements we encounter are (1) an overview or inventory for a region and (2) a local analysis of one or a few landslides. In both cases, the historic analysis is a key element. Data from the institutional SAR missions with rich and accessible archives are therefore mainly used, e.g., Sentinel-1 [2], which acquires images over most of Europe every 6/12 days in both ascending and descending orbits since 2014. While satellite InSAR can also provide a relevant contribution to the monitoring of fast and potentially accelerating landslides, very often terrestrial radar measurements [3-5] are preferred in this case due to their higher flexibility and fast access to the information

In this work we specifically address the use of ALOS-2 PALSAR-2 L-band ScanSAR for the landslide application. At L-band, the wavelength is more than 4 times longer than at C-band. The longer wavelength results in a lower phase to displacement sensitivity. For a given phase noise, this results in a lower displacement rate precision, given that the number of acquisitions and the acquisition dates are the same. However, this also means that faster displacements can potentially be included into the result and that the coherence over vegetated areas is higher, as has already been confirmed using JERS [6] and ALOS PALSAR [7] data.

Considering the ALOS-2 PALSAR-2 archive over Switzerland, we find that suitable stripmap mode data stacks were systematically acquired only for the ascending orbit. For the descending orbit, suitable stripmap mode data stacks were only acquired over specific areas. When considering ScanSAR acquisitions, we found that suitable data stacks were indeed acquired over the entire Swiss Alps, in particular in descending orbit. Given the 350 km swath width of the ScanSAR data, the entire Swiss Alps can be covered in a single acquisition, which is very attractive in the processing of a survey type product (Figure 1). L-band ScanSAR interferometry has already been demonstrated using PALSAR data [8]. To obtain coherence, synchronized bursts are required. While this was not always the case for PALSAR data, the PALSAR-2 ScanSAR data are synchronized since 2015 and thus interferometry works well. Both Differential Interferometric SAR (DInSAR) and Persistent Scatterer Interferometry (PSI) can be successfully applied to burst-synchronized PALSAR-2 ScanSAR data [9,10].

Section 2 describes some data characteristics and the DInSAR processing strategy. Section 3 outlines the PSI strategy. The results are discussed in Section 4, followed by conclusions and outlook in Section 5.

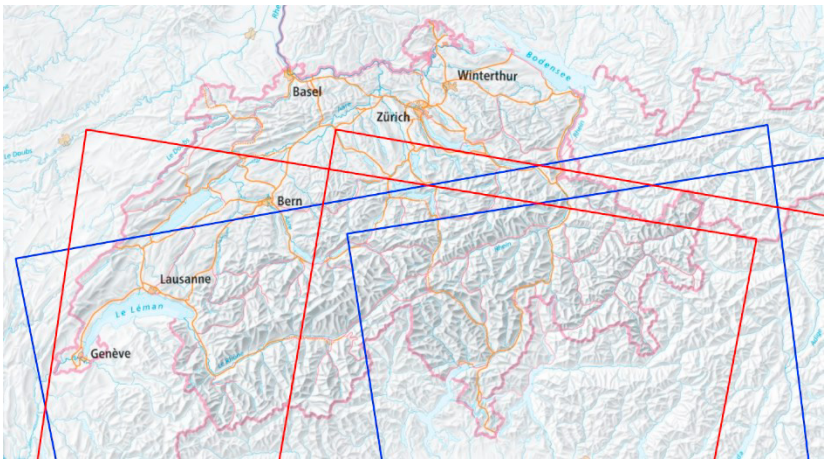


Fig. 1. ALOS-2 PALSAR-2 ScanSAR ascending (blue) and descending orbit (red) coverage over Switzerland (Background Map © swisstopo 2023.

2. PALSAR-2 ScanSAR DInSAR

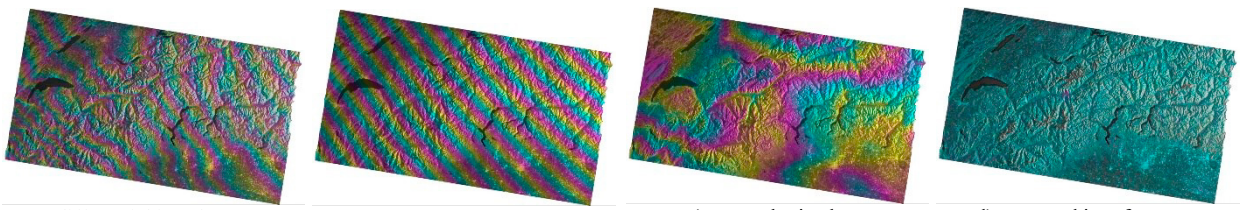
Two PALSAR-2 ScanSAR SLC products are available, either from burst or full aperture processing. The SLC product obtained from the burst processing provides the SLC data per burst. A relevant practical advantage of this product is its smaller file size. In the azimuth direction the bursts overlap significantly, where each point on the ground

is covered by about 5 bursts. In principle InSAR is possible with this SLC product, but we observed phase anomalies for some bursts that could not be resolved. We therefore used the full aperture processing SLC product. Here, the azimuth sampling is fine enough to sample the entire spectrum covered by the 5 bursts over an area. Only about 20% of the azimuth spectrum is effectively used, resulting in a large file size, yet using the phase information is straight forward and reliable. PALSAR-2 is operated in a relatively small orbital tube, with baselines clearly below 1 km.

The PALSAR-2 ScanSAR Wide Beam acquisitions include five sub-swaths. The resulting full aperture SLC consists of five sub-swath SLC data sets. Per sub-swath, differential interferograms can be generated in slant-range geometry, geocoded, and then mosaiced into one large differential interferogram in map geometry. Using our orbit-based simulation of the topographic and orbital phase, we find that the differential interferometric phases are consistent between the five sub-swaths, as was demonstrated e.g., in [9]. The alternative processing method used here is to resample the sub-swath full aperture SLCs to a common grid so that they can be treated as a "normal burst SLC" with only a single burst but multiple sub-swaths. This method permits using our available tools for burst SLC data (such as Sentinel-1 TOPS mode data or Radarsat Constellation Mission ScanSAR data), which facilitate subsequent steps, such as co-registration, multi-looking, cutting between sub-swaths, and mosaicking in slant-range geometry. As a result, a co-registered mosaic SLC stack is available, that can be largely used in the same way as a stack of co-registered stripmap mode data. Using available mosaiced SLCs in slant-range geometry may be an advantage for certain processing tasks, such as the identification and mitigation of ionospheric effects, the estimation and removal of phase trends which are linear in the slant-range geometry, and the combined use of ScanSAR and stripmap data [10]. A more practical advantage is that there are significantly fewer files.

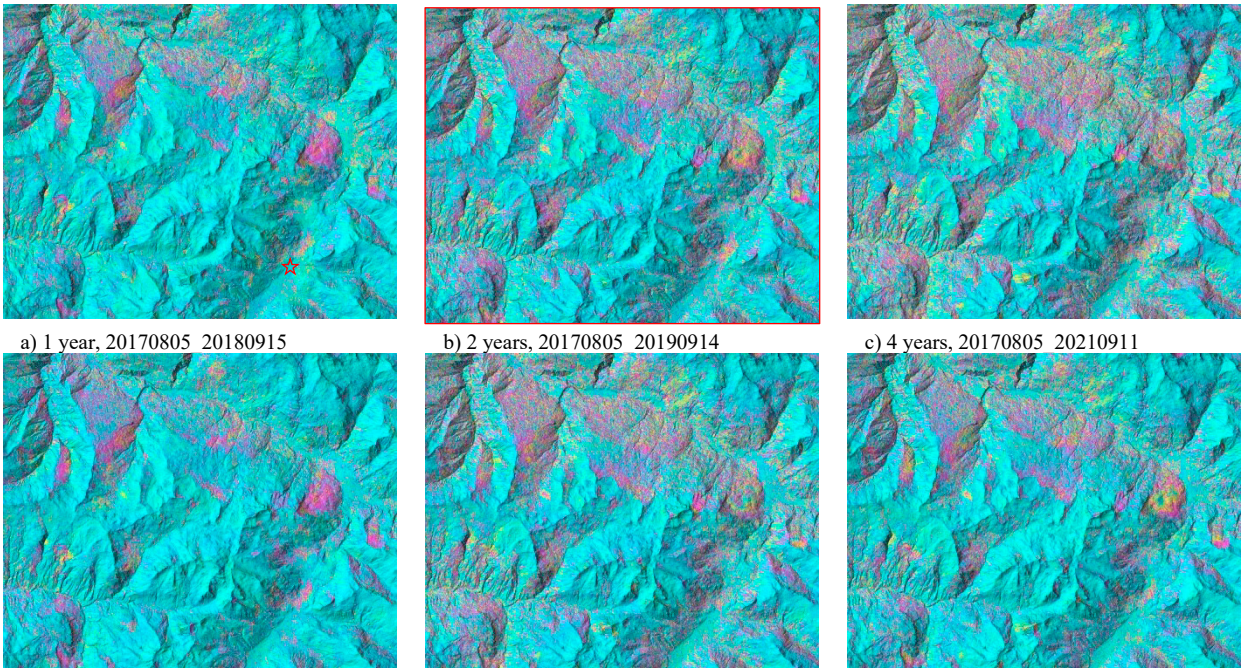
A geocoded PALSAR-2 ScanSAR differential interferogram over Switzerland is shown in Figure 2. After subtracting a linear phase ramp and an atmospheric phase model, the resulting phase is overall close to zero. Local deviations primarily relate to ground-motion, while phase noise relates to decorrelation. As shown in Figure 2, the phase ramp is significant for early acquisitions and much smaller for later data. This is most likely related to the raw data focusing and updates to the processor used. The estimated atmospheric phase includes a stratigraphic part, for which a linear dependence on the topographic height is assumed, together with a spatially dependent term estimated by smoothing the phase using a large spatial filter.

Figure 3 shows PALSAR-2 ScanSAR differential interferograms over an area including Davos, Switzerland. Landslide displacement signals clearly scale with the time interval. Some of the visible landslides, such as the Gotschna landslide to the right of the image center, include forested areas. For differential interferograms with comparable time intervals the phases look similar. For pairs with three- or four-year time intervals, the phase becomes increasingly noisy due to temporal decorrelation. Over faster moving landslides, such as the Moosfluh landslide along the Great Aletsch Glacier (Figure 4), differential interferograms are also of high interest, as they may provide information in areas where Persistent Scatterer Interferometry fails. For some slower landslides, the longer interval pairs are relevant to reliably identify and delineate the moving area and estimate its displacement velocity.



a) differential interferogram b) linear phase ramp c) atmospheric phase d) corrected interferogram

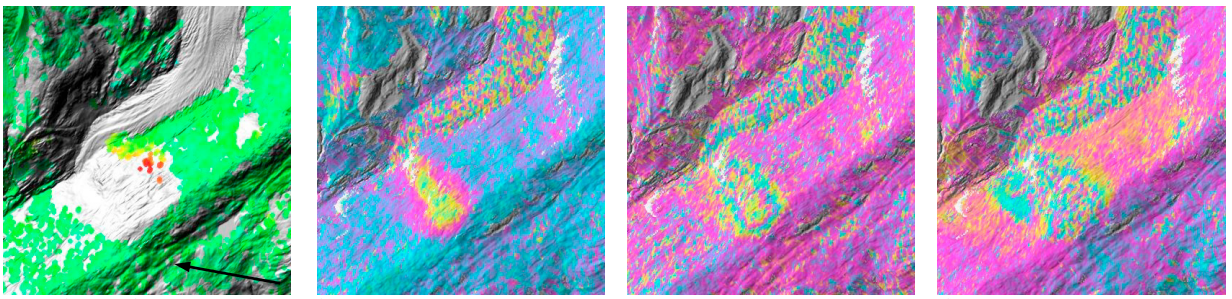
Fig. 2. Geocoded PALSAR-2 ScanSAR differential interferogram (descending orbit, 25-Jun-2015 to 23-Jul-2015) over Switzerland. From the initial differential interferogram (a), a linear phase ramp (b) and the estimated atmospheric phase (c) are subtracted to get the corrected differential interferogram shown in (d). One color cycle corresponds to one 2π phase cycle.



a) 1 year, 20170805_20180915 b) 2 years, 20170805_20190914 c) 4 years, 20170805_20210911

d) 1 year, 20180915_20190914 e) 3 years, 20180915_20210911 f) 2 years, 20190914_20210911

Fig. 3. Geocoded, trend- and atmosphere-corrected PALSAR-2 ScanSAR differential interferogram sections (ascending orbit, 10km x 8 km) over Davos (red star in a), Switzerland, with time intervals between one and four years. One color cycle corresponds to one 2π phase cycle, respectively to a line-of-sight displacement of 12cm. Dates are indicated in the format yyyymmdd.



a) desc. path 95 PSI result b) DInSAR 20150723_20150903 c) DInSAR 20150723_20151015 d) DInSAR 20150723_20160623

Fig. 4. Descending orbit PALSAR-2 ScanSAR PSI (a, same scale as Figure 5) and DInSAR (b,c,d, one color cycle corresponds to one 2π phase cycle) results over the Moosfluh landslide. PSI results show a large gap at the location of the Moosfluh landslide, indicating that phase unwrapping over this relatively fast and non-uniformly moving area could not be resolved. The displacement phase in the differential interferograms is clearly visible for the shorter time intervals of 42 (b) and 84 (c) days, indicating that the velocity is roughly 10cm/month. Over a period of almost one year (d), the phase looks noisy due to decorrelation and phase wrapping.

3. PALSAR-2 ScanSAR Persistent Scatterer Interferometry

Multi-temporal stacks of co-registered PALSAR-2 ScanSAR mosaic SLCs can be used for PSI and other interferometric time series analysis methods. The PALSAR-2 ScanSAR acquisition stacks covering Switzerland and used in this work are the descending paths 94 and 95 and ascending paths 198 and 199 (Figure 1). To avoid low coherence and phase effects from snow cover, especially at higher elevations, we exclude winter and spring acquisitions. The resulting stacks are relatively small with less than 15 scenes between 2015 and 2021 for the descending orbits and less than 10 scenes for the ascending orbits.

For the identification of persistent scatterer (PS) candidates, we mainly used the spectral diversity criteria. The total azimuth spectrum width of the full aperture SLCs is larger than that of the stripmap mode data, while the range bandwidth is about half of that of the stripmap mode data. Consequently, the method is well suited for the identification

of point-like scatterers. This is important considering that only small data stacks were available and thus the identification of PS candidates based on the temporal backscatter variability is not very reliable. Furthermore, it is important that a large fraction of the PS candidates are suitable candidates to be included in the solution. For small data stacks, the regressions in the time series processing include only few points. Consequently, the regression statistics are less reliable than for large data stacks, making it more relevant to check the spatial consistency of the solution and remove outliers.

For Switzerland, we used the SwissAlti3D (© swisstopo 2021) digital elevation model (DEM) as a topographic reference. Due to this high-quality terrain model and the short spatial interferometric baselines for PALSAR-2, an estimation of the point height corrections was not necessary. Using one-dimensional instead of two-dimensional regressions ensured that the process was more robust and faster. This was further supported by the estimation and removal of overall phase trends and the main atmospheric path delays. Because of the L-band frequency, the phase noise, atmospheric path delay variation, and sensitivity to height errors and displacements are all relatively low. As a result, the technique worked well, in spite of the small stacks available.

The displacement rate estimation precision was also determined. It depends strongly on the total time period covered, as well as on the number of acquisitions available for that period, and the phase deviation thresholds used in the processing. For the larger descending orbit stacks the displacement rate estimation precision values were mostly < 1.5mm/year and for the small ascending orbit stacks mostly < 3.5mm/year.

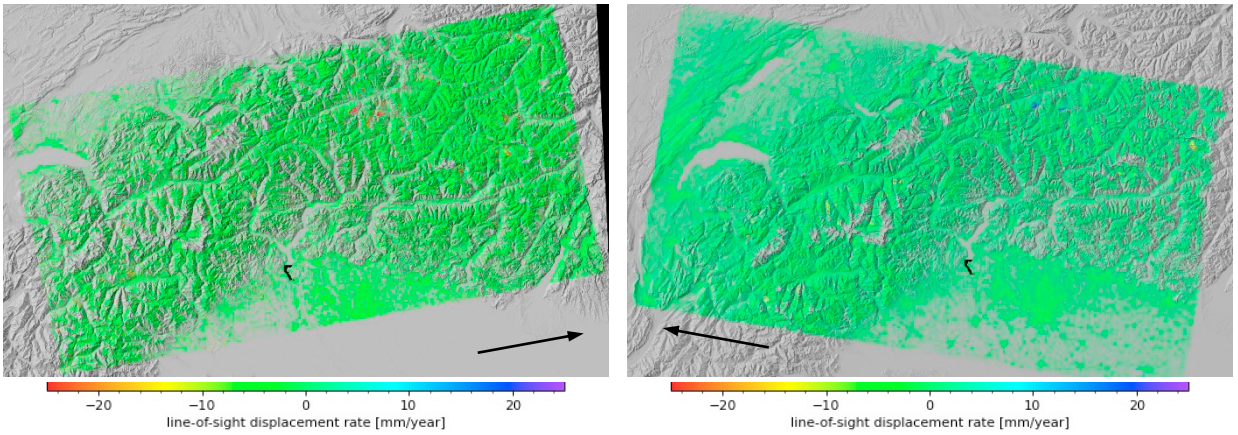
The coverage of the processed PALSAR-2 ScanSAR sections is up to 70’000 km^2, which also means that a very large number of PS candidates need to be used. To keep the PS candidates list sizes below 100 million points, we applied an adaptive point density reduction that primarily reduces the point density in areas with a high density [12]. This step also permitted avoiding “redundant copies” of persistent scatterer results in adjacent azimuth pixels, which are otherwise observed because of the azimuth oversampling of the full aperture ScanSAR SLCs. For a primarily alpine area, the final point density of the results of approx. 300 points/km^2 was quite high.

For selected areas, a local reprocessing was done to further increase the point density, consolidate the result through the use of a closer reference point, and more carefully check the phase unwrapping and resulting displacement result.

Through the use of two ascending and two descending orbits, we obtained more than one result for much of the Swiss Alps. This in turn allows for a validation procedure, as the identification of a landslide in two independent results increases the overall certainty of the result.

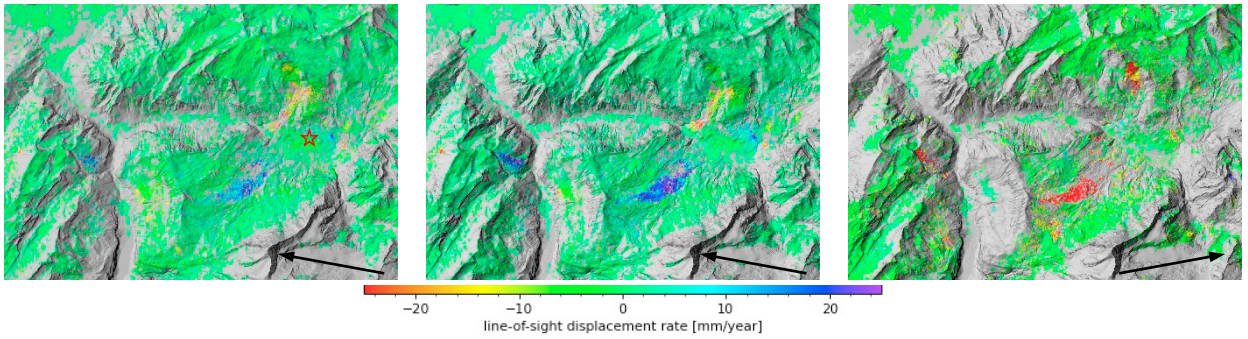
4. Landslide results in Switzerland

The large swath width of the PALSAR-2 ScanSAR data enables the coverage of almost the entire Swiss Alps in a single acquisition geometry. Figure 5 shows an overview of the results obtained in the PSI processing for the main ascending and descending paths over Switzerland. An intercomparison of the results together with results obtained using other SAR satellites and with information from other sources indicates that most known landslides are reliably identified. Due to the longer L-band wavelength, the potential to identify faster movements (> 2cm/year) and movements in vegetated areas is clearly higher than at C- or X-band. A more detailed view of the result is shown in Figure 6 for the Grindelwald area. Several landslides of different sizes, motion directions and velocities are identified. The result also includes information for vegetated and forested areas (Fig. 7).



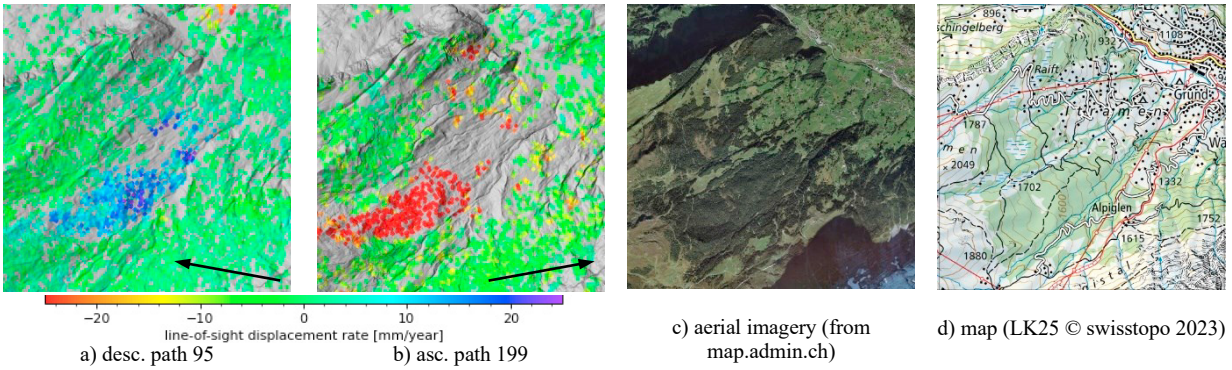
a) asc. path 199 b) desc. path 95

Fig. 5. Ascending (a) and descending (b) orbit PALSAR-2 ScanSAR PSI line-of-sight displacement velocity maps over Switzerland. The East-West extent of the area shown is more than 380km. The black arrow indicates the line-of-sight direction. The ascending orbit geometry is better suited for the western side of valleys, the descending orbit geometry for the eastern side. Line-of-sight displacement rates up to about 7cm/year are observed.



a) desc. path 95 b) desc. path 94 c) asc. path 199

Fig. 6. PALSAR-2 ScanSAR PSI results over Grindelwald (red star in a), Switzerland. The size of the area is 20km x 14km. There is a good consistency between the results. The black arrows indicate the line-of-sight direction.



a) desc. path 95 b) asc. path 199 c) aerial imagery (from map.admin.ch) d) map (LK25 © swisstopo 2023)

Fig. 7. Ascending (a) and descending (b) orbit PALSAR-2 ScanSAR PSI line-of-sight displacement velocity maps for Itramen, Switzerland. The comparison with the aerial photo (c) and the topographic map (d) clearly confirm that the coverage also includes forested areas. The size of the area is 5km x 5km. The black arrow indicates the line-of-sight direction. The fastest displacements observed in the result are around -45 mm/year.

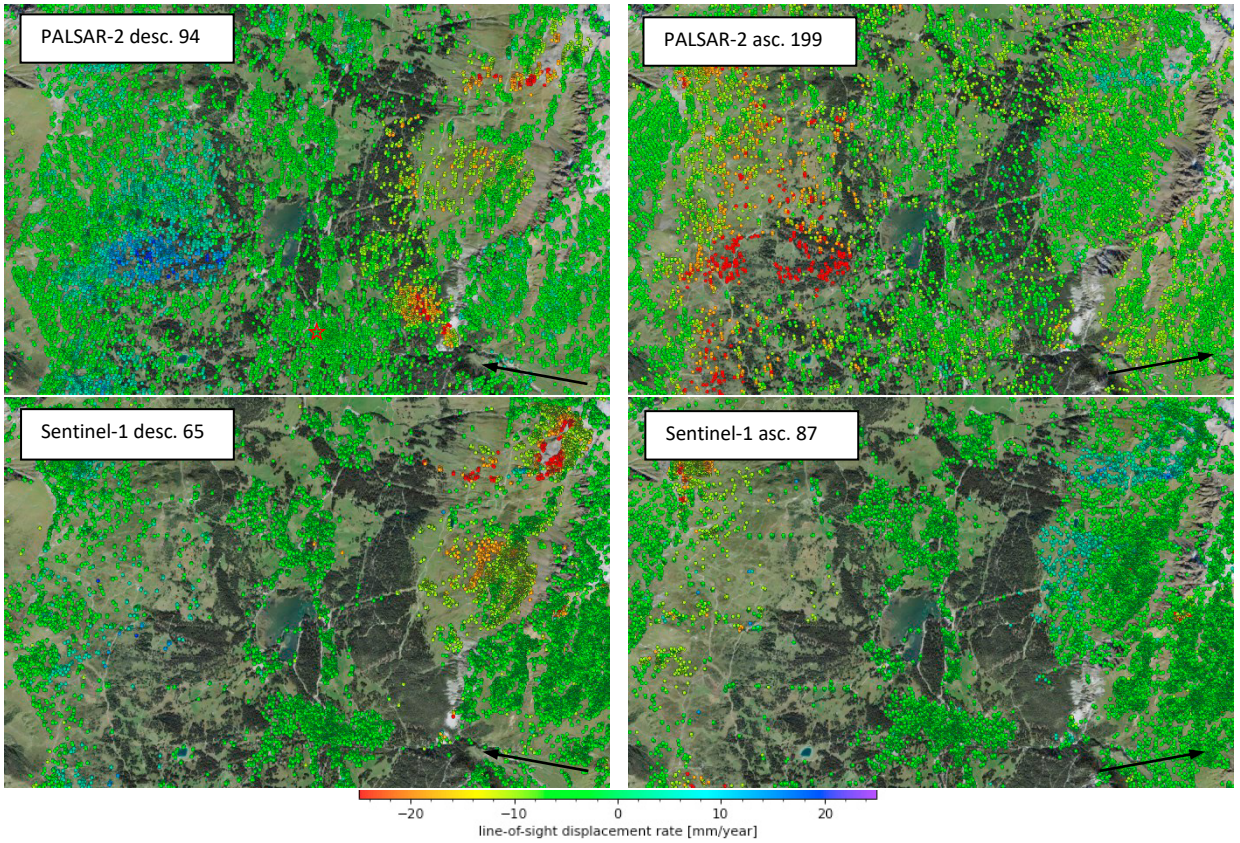


Fig. 8. Ascending (right) and descending (left) orbit PALSAR-2 ScanSAR (top) and Sentinel-1 (bottom) PSI line-of-sight displacement velocity maps for Lenzerheide, Switzerland. The results clearly confirm that the PALSAR-2 results also include forested areas, which is not the case for the C-band Sentinel-1 result. As a result the landslides in the area are much better identified and characterized at the longer L-band wavelength. The width of the area shown is 7km. The black arrow indicates the line-of-sight direction. Image background: SWISSIMAGE © swisstopo 2023.

For Switzerland, the better coverage achieved at L-band for vegetated areas is a relevant advantage compared to previous C-band results, which were limited more or less to built-up areas and the high alpine zone above the tree line. Satellite L-band interferometry performs well in the pre-alpine areas, as shown in Figure 8 for Lenzerheide, Switzerland. Additionally, landslides on vegetated slopes are better identified in L-band compared to C-band.

A local reprocessing can be applied for selected areas of interest to further increase the point density, consolidate the result with a more local reference point, and more carefully check the phase unwrapping and resulting displacement maps.

5. Conclusions and Outlook

In this work we confirmed that ALOS-2 PALSAR-2 ScanSAR data are suitable for differential interferometry and interferometric time series analysis methods such as PSI. Relatively small data stacks over Switzerland were used to map ground motion. Relevant displacement rates (> 0.5 cm/year) were primarily found in the pre-alpine and alpine regions.

Particular strengths relating to the lower L-band frequency of approx. 1.2 GHz include (1) the possibility to conduct a time-series analysis with a small data stack of about 10 images within eight years, (2) the potential to identify, map and quantify displacement rates > 2cm/year, and (3) the potential to map ground displacement in vegetated and even forested areas. For L-band stacks of more than 10 scenes and with a total coverage of at least 4 years the statistical displacement rate estimation error was below 3mm/year for more than 90% of the points. Overall, the processing

proved to be quite robust, in spite of the small stacks used. In addition to the lower L-band frequency, the relatively short baselines, accurate orbit information and high-quality DEM contributed to this.

Differential interferograms also provide useful information on ground motion. They can be considered for higher motion rates of several dm/year, yet the interpretation of the somewhat noisy geocoded differential interferograms requires some experience. Furthermore, the spatial resolution is lower for ScanSAR than for stripmap data.

The availability of suitable satellite SAR data will strongly improve in the near future with the L-band mission plans of NASA/ISRO, ESA, JAXA and others (see Table 1). The NISAR and ROSE-L missions both foresee frequent L-band repeat-pass observations similar to the current Sentinel-1 C-band mission. One strong aspect of the Japanese PALSAR-3 L-band SAR on ALOS-4 is that it will be operated in the exact same orbits as PALSAR-2. Consequently, displacement time series can be continued.

Table 1. Institutional L-band SAR mission plans. Further national L-band missions are also planned or in operation, e.g. the SAOCOM L-band mission of Argentina with 2 L-band SAR satellites in operation.

Satellite/Mission	Frequency	Acquisitions	Data access	Launch	Remarks
NASA-ISRO NISAR https://nisar.jpl.nasa.gov	L-band: 24 cm S-band: 9 cm	Global every 12 days S-band over India	Free and open	2024	Orbit tube < 500m Mission 3 – 5 years Resolution 3-10m
ESA ROSE-L	L-band	12-days repeat orbit	Free and open	2028	Copernicus mission Mission 7.5 years Successor planned
JAXA PALSAR-3	L-band	14-days repeat orbit (same as PALSAR-2)	AO Projects	2023 / 2024	Successor of PALSAR-2

Acknowledgments

This work was supported by the EUROSTARS Project E!113220 RAMON (EUREKA, co-financed by Innosuisse) and the JAXA Projects ER2A4N001 and ER3A4N003. Sentinel-1 data copyright ESA/Copernicus 2023.

References

[1] Wegmüller, U.; Caduff, R.; and T. Strozzi: Einsatz von Radarmethoden im Geomonitoring der Schweiz. In: Tagungsband Geomonitoring 2020, S. 3-15. DOI: https://doi.org/10.15488/9336

[2] ESA Webpage for Sentinel-1, 2023; https://sentinel.esa.int/web/sentinel/user-guides/sentinel-1-sar

[3] Caduff, R., Schlunegger, F., Kos, A., & Wiesmann, A. (2014). A review of terrestrial radar interferometry for measuring surface change in the geosciences, Earth Surf. Processes Landforms, 02/2015; 40(2). DOI:10.1002/esp.365.

[4] Kos A., F. Amann, T. Strozzi, R. Delaloye, J. von Ruette and S. Springman, Contemporary glacier retreat triggers a rapid landslide response, Great Aletsch Glacier, Switzerland, Geophys. Res. Lett., 43, doi:10.1002/2016GL071708, 2016.

[5] Caduff R. and T. Strozzi, Terrestrial radar interferometry monitoring during a landslide emergency 2016, Ghirone, Switzerland. In: Mikoš M, Arbanas Ž, Yin Y, Sassa K (eds) Advancing culture of living with landslides, vol 3. p 301-309. Springer Int. Publ., Switzerland, 2017.

[6] Strozzi T., P. Farina, A. Corsini, C. Ambrosi, M. Thüring, J. Zilger, A. Wiesmann, U. Wegmüller, and C. Werner, Survey and monitoring of landslide displacements by means of L-band satellite SAR interferometry, Landslides, Vol 2, Nr. 3, pp 193-201, Oct. 2005.

[7] Strozzi, T., Wegmüller, U., Werner, C., Wiesmann, A., Santoro, M., Delaloye, R., Raetzo, H., Ambrosi, C., „Survey of landslide activity in the Swiss Alps with ALOS PALSAR," Proceedings of ALOS PI 2008 Symposium, Rhodos, 3-7 November, SP-664, CD-ROM, 2008

[8] Werner C., U. Wegmüller, O. Frey, and M. Santoro, „Interferometric processing of PALSAR Wide-Beam ScanSAR data," Proc. Fringe'11, Frascati, Italy, 19. – 23. Sep. 2011.

[9] Strozzi T., D. Carreon-Freyre, and U. Wegmüller, "Land subsidence and associated ground fracturing: study cases in central Mexico with ALOS-2 PALSAR-2 ScanSAR Interferometry," Proc. IAHS Tenth International Symposium on Land Subsidence (TISOLS), 382, 179-182, 2020.

[10] Strozzi T., R. Caduff, N. Jones, A. Manconi, and U. Wegmüller, "L-Band StripMap-ScanSAR Persistent Scatterer Interferometry in Alpine Environments with ALOS-2 PALSAR-2," in Proc. IEEE Int. Geosci. Remote Sens. Symp., 2022, pp. 1644–1647. https://doi.org/10.1109/IGARSS46834.2022.9884743.

[11] Wegmüller U., C. Werner, T. Strozzi, and A. Wiesmann, „Multi-temporal interferometric point target analysis", in Analysis of Multi-temporal remote sensing images, Smits and Bruzzone (ed.), Series in Remote Sensing, Vol. 3, World Scientific (ISBN 981-238-915-61), pp. 136-144, 2004.

[12] Wegmüller U., O. Frey, and C. Werner, „Point Density Reduction in Persistent Scatterer Interferometry", Procs. EUSAR 2012 Conf., 24-26. Apr. 2012.